



PERGAMON

Continental Shelf Research 22 (2002) 1987–2000

CONTINENTAL SHELF  
RESEARCH

www.elsevier.com/locate/csr

# The accumulation and decay of near-bed suspended sand concentration due to waves and wave groups

Christopher E. Vincent<sup>a,\*</sup>, Daniel M. Hanes<sup>b</sup>

<sup>a</sup>*School of Environmental Sciences, University of East Anglia, Norwich NR4 7TJ, UK*

<sup>b</sup>*Department of Civil and Coastal Engineering, University of Florida, PO Box 116590, Gainesville, FL 32611-6590, USA*

Received 2 August 2001; received in revised form 2 May 2002; accepted 8 May 2002

## Abstract

High resolution acoustic measurements were made of suspended sand and bedform dimensions caused by prototype-scale waves, both regular and in groups, over a mobile sand bed, in a very large wave channel. The changes in wave height at the beginning of the regular waves and within wave groups provides an opportunity to examine the time lag in the response of the sediment. For regular waves suspended sand concentrations lagged the forcing waves with the lag increasing with distance from the seabed. Typically, near-bed (1–2 cm) concentrations reached an equilibrium one to two wave-periods after the waves themselves had reached their steady height while at elevations of 10–15 cm the lag was longer. This lag was interpreted as due to the continual injection of turbulence into the water column from vortex processes associated with the oscillatory wave boundary layer over bedforms. A similar pattern was seen for wave groups, with the sand concentration near the bed lagging by the waves by one to two wave-periods and increasing with distance from the bed. Despite the controlled nature of these prototype-scale suspension experiments, with detailed measurements of bedforms and attempts to achieve ‘equilibrium’ bedforms, considerable variability ( $\pm 30\%$ ) in the suspended sand concentration occurred between ‘similar’ forcing conditions, both at a wave-to-wave level and on the scale of groups and longer. The results suggest that considerable variability (a factor of two or more) should be expected in the suspension due to turbulence produced from wave boundary layers in natural environments, where bedforms are frequently continually evolving as the waves change their height, period and direction.

A simple wave-average suspended-load model is used to describe the major temporal features of the suspension and to quantify the lag of the suspended sediment in relation to the waves and wave groups. Quantification of the lag is essential for assessing the transport of sand at infra-gravity frequencies. A decay rate of  $0.06 \text{ s}^{-1}$ , applied to antecedent waves, decreased the mean average error (MAE) by a factor of 3 when predicting the suspended load of the repeating wave groups. When tested against five further data sets (including random waves and wave records from the SANDYDUCK field experiment) including the decay rate of  $0.06 \text{ s}^{-1}$ , resulted in a decrease in the MAE of a factor of 1.5–2 (compared to the same model with no lag). The entrainment (pickup) constant in the same model was variable and no consistent pattern was found, although there were suggestions of a link to the location of the measured profile relative to the bedforms. © 2002 Elsevier Science Ltd. All rights reserved.

*Keywords:* Waves; Groups; Sand; Resuspension; Bedforms; Entrainment

## 1. Introduction

The suspension of sand by waves is a non-linear process; suspension does not depend simply on the

\*Corresponding author. Fax: +44-1603-507719.

E-mail addresses: c.vincent@uea.ac.uk (C.E. Vincent), hanes@ufl.edu (D.M. Hanes).

height of the wave. In addition to factors such as sand size, bedforms, etc., it also depends on the heights of antecedent waves. This dependency on previous waves is immediately clear from the examination of any detailed suspension record where it will be noted that, as a wave group passes, the suspension associated with a wave later in the group is much higher than that due to a wave early in the group, although they may have the same height (Hanes, 1991; Villard et al., 1999). The effect is one of sediment being pumped-up through the water column, each wave adding more turbulence (and supporting more suspended sand) before that from the previous wave has dissipated. This lag in suspension can result in significant sand transport at infra-gravity frequencies (e.g. Vincent et al., 1999) although the suspension itself is mainly an incident-wave process rather than an infra-gravity-wave process.

One of the objectives of the Small-scale International Sediment Transport Experiment (SISTEX99), conducted in the large wave channel of the Forschungs Zentrum Küste (FZK) in Hannover, was to examine the pumping-up of sediment by waves and wave groups under controlled, prototype-scale conditions over bedforms of known dimensions in deep, mobile sand. Details of the SISTEX99 can be found in Ribberink et al. (2000).

## 2. The SISTEX99 experiment

Laboratory experiments were conducted in the wave channel at the FZK in Hannover, Germany between June and September 1999. The channel is 300 m long, 5 m wide and 7 m deep. A sand bed, 45 m long and 0.7 m thick, was installed in the bottom of the channel approximately 100 m from the wave generator. The sand was held in place at each end by 15 m-wide immobile sections. The sand used was well-sorted quartz sand with a sieved  $D_{50}$  of 0.24 mm. The fall velocity distribution by weight was independently and directly measured, giving a median fall velocity of  $3.6 \text{ cm s}^{-1}$ . Waves were generated by a wave-paddle with dynamic feed-back control to reduce reflected and trapped waves. At the far end of the

channel a beach ( $6^\circ$  steepness) also absorbed the wave energy. Wave-wires to measure water surface elevations were spaced along the channel. Instruments were mounted on frames cantilevered out 1 m from the channel wall close to the middle of the sand bed and directly in line with wave-wire 13. The instruments referred to in this paper were the 2.4 m-long multiple transducer array (MTA), a 3-transducer ABS system (2, 4, 5 MHz) mounted close to the MTA with its transducers spaced horizontally to allow suspension profiles over different parts of the bedform to be measured simultaneously, two acoustic Doppler velocimeters (ADV), a pressure sensor, and an electromagnetic current meter. The MTA (Hanes et al., 2001; Jette and Hanes, 1997) consisted of three segments, the centre section (50 cm long) having 32 transducers while the two outer sections (90 cm long) each had 16 transducers. The ADV measurement volumes were approximately 10–15 cm above the bed, and located near the centre of the MTA. The two-component Valeport discus-head electromagnetic current meter at 0.5 m above the bed was cantilevered from the other wall of the channel, exactly opposite the centre of the MTA and wave-wire 13. A mobile carriage running along the top of the channel was used to take bed profiles along the axis of the channel between wave runs, using a second, shorter MTA. The carriage was also used to make suction samples of the time-averaged suspended sand concentration in the centre of the channel while waves were being generated; suspended sand size was observed to decrease with height above the bed, at 0.1 m  $D_{50}$  decreased to 0.19 mm over rippled beds and to 0.10 mm over a flat beds. Further details of the FZK channel and instrumentation can be found in Ribberink et al. (2000).

The wave channel was filled to a depth of 4.75 m (4 m above the sand bed); the sand bed had been raked flat prior to filling the tank. The water used to fill the channel came from a nearby canal and contained considerable fine sediment so visual or video monitoring of the sand bed was not possible. Overnight this sediment would settle into a layer 1–2 mm thick on top of the sand bed (viewed through an observation window in the side of the channel). The water was very turbid throughout

the experiment but the effect on ABS backscatter signal was small relative to that from sand (Green et al., 1999). A number of different waves were generated, ranging from regular (monochromatic) waves to ‘real’ waves reproduced from a time series of water elevations from Duck, North Carolina (obtained during the SANDYDUCK field experiment in 1997), and the sand suspension and bedform evolution was investigated. In this paper, we examine the results from monochromatic waves and repeating wave groups.

### 3. Results

#### 3.1. Monochromatic waves

Monochromatic waves of period 6.5 s and nominal heights of 0.55, 1.0, 1.3 and 1.6 m, were generated. In each case waves of a given height were generated for two 30-min periods. After the second 30-min ‘run’ for each wave condition a profile of the sand bed along the centre of the channel was obtained using the MTA on the mobile carriage. The first 30-min run allowed the sand bed to establish an ‘equilibrium’ profile with the waves. The waves usually reached their design height by the fourth wave. The actual heights were calculated from the water level excursions from wave wire 13.

##### 3.1.1. Bedforms and suspension

Time-series of sand suspension indicate that equilibrium is generally reached in about 10–20 min (100–200 waves). Although bedforms may migrate, there is usually no statistical difference between their shapes after 30 and 60 min. Fig. 1a shows the bed profile beneath the MTA at the beginning of the second 30-min run of waves of each height (solid line) and the profile 15 min later (dashed line). For the three higher wave conditions the wavelengths of the bedforms  $\lambda_b$  increase with the orbital excursion  $D_0$  (Table 1) and are consistent with  $\lambda_b = 0.6D_0$  (Miller and Komar, 1980). Average concentration profiles at the beginning of each run (calculated from waves 7–15) are shown in Figs. 1b and c, and represent the equilibrium concentrations reached after

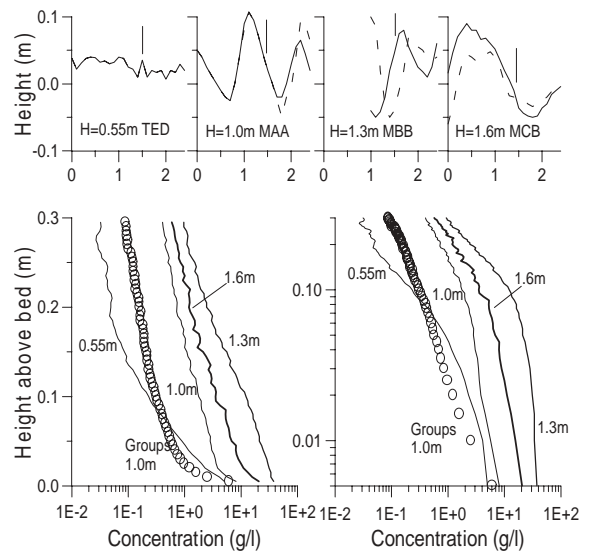


Fig. 1. (a) Top: MTA bedform profiles beneath the ABS transducers for 4 monochromatic waves (scale is in metres). The solid lines are the profiles at the beginning of the runs, the dashed lines are the profiles 15 min later. The vertical line indicates the position of the ABS transducer. 1 (b) Lower left: Average concentration profiles for the same 4 monochromatic waves at the beginning of each Run (waves 7–15), together with the group-average profile ( $H_s = 1.0$  m Run GAA) for comparison, plotted on log-linear axis. 1 (c) Lower right: The same profiles plotted in log-log space.

pumping-up by an ‘infinite’ group. The profile shapes follow the simple exponential decay with height suggested by the Nielsen (1992) pick-up vortex-ejection model; this is a straight line on Fig. 1b given by

$$C(z) = C_{ref} \exp(-z/l), \quad (1)$$

where  $C_{ref}$  is the concentration at height  $z = 0$  (a reference concentration) and  $l$  is a mixing height. Fig. 1c shows the same profiles plotted in log-log space (a straight line line would indicate a diffusive-type Rouse suspension process). Close to the bed (within  $\sim 5$  cm) the profiles for the higher waves also fit the Rouse-shape suggesting that sheet-flow may occur over the surface of the larger bed-forms (of the type observed by Green and Black (1998) in video recordings made over hummocky bedforms in 15 m water depth off the coast of New Zealand).

Table 1

Design wave heights and wave heights ( $H_{rms}$ ) calculated from the wave-wire excursion. The orbital water speed  $U_w$  and the orbital excursion are those from first-order wave theory. Bedforms are from the MTA at the location of the ABS sensors

Run ID	Design $H_t$ (m)	$H_{rms}$ (m)	$U_w$ ( $\text{m s}^{-1}$ )	Orbital exc $D_0$ (m)	Local MTA bedforms	
					Height (cm)	Length (m)
TED	0.55	0.58	0.38	0.82	0.5–2	0.2
MAA	1.0	1.07	0.68	1.48	12	0.95
MBB	1.3	1.40	0.89	1.92	20	2–3
MCB	1.6	1.72	1.09	2.37	10	2.2–3

The decrease in suspended sand concentrations when the waves increased in height from 1.3 to 1.6 m was due to a decrease in the height of the bedforms. The likely explanation was that the ‘break-off’ point (Grant and Madsen, 1982) had been exceeded and the bedforms were less steep for the larger wave conditions. Our local bedform profiles indicate that the bedform slope for the larger waves was about 50% less than the bedform slope for the smaller waves.

### 3.1.2. Sediment pumping

The pumping-up of sediment by the waves can be seen at all 4 wave heights. Two examples are shown here: the lowest suspension condition with  $H = 0.55$  m (Fig. 2) and the highest suspension  $H = 1.3$  m (Fig. 3). In both of these diagrams the instantaneous currents 0.5 m above the sand bed are shown at the top. The suspension time series and the profiles are wave-average values corresponding to the waves indicated on the instantaneous current time series (a wave being defined from one current zero up-crossing to the next). Close to the bed (1–2 cm) the concentrations closely follow the wave magnitude, tending to lag by about one to two waves. Higher in the water column the lag tends to increase. The relatively uniform concentration between 10 and 20 cm for profiles 3–5 in Fig. 2 is probably associated with the upward dispersal of the mud from the bed. The vertically integrated suspended load (between 0.005 m and 0.30 m) is also shown.

Also noteworthy is the wave-to-wave variability of sediment concentration at all heights (a factor of 2 close to the bed, a factor of 5 at higher elevations); this may be due to subtle changes in

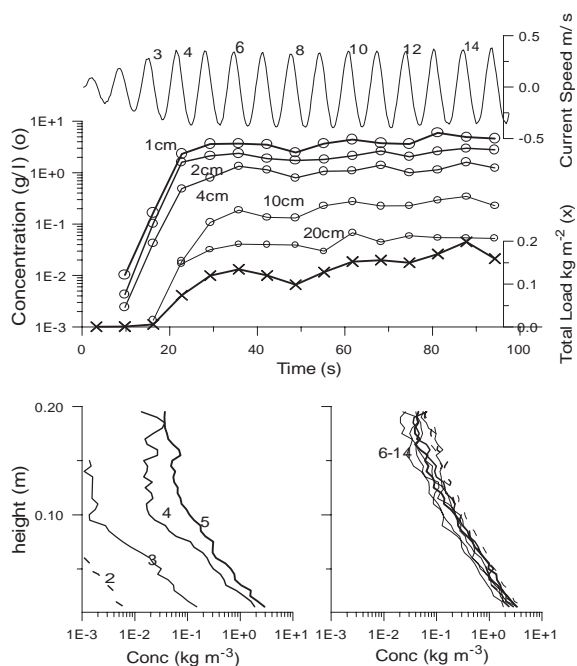


Fig. 2. Top: Current speed 0.75 m above the sand bed for the first 15 waves for Run TED with  $H = 0.55$  m. Middle: Time series of wave-average concentrations ( $\circ$ ) at 1, 2, 4, 10 and 20 cm above the bed and total suspended load ( $\times$ ). Note the tendency for a 1 wave lag at the lowest heights and the 2-or-more wave lag higher above the bed. Bottom: Sequence of wave-average concentration profiles showing the changes in the profile shape. Numbers refer to the waves in the top diagram.

the waves or the bedforms but are not predictable from our data. The standard deviation in the suspended load, after the waves have reached full height, is typically  $\pm 30\%$ , while the standard deviation in the wave height is  $\pm 4\%$ , and the variations in concentration and wave height are not correlated with each other.

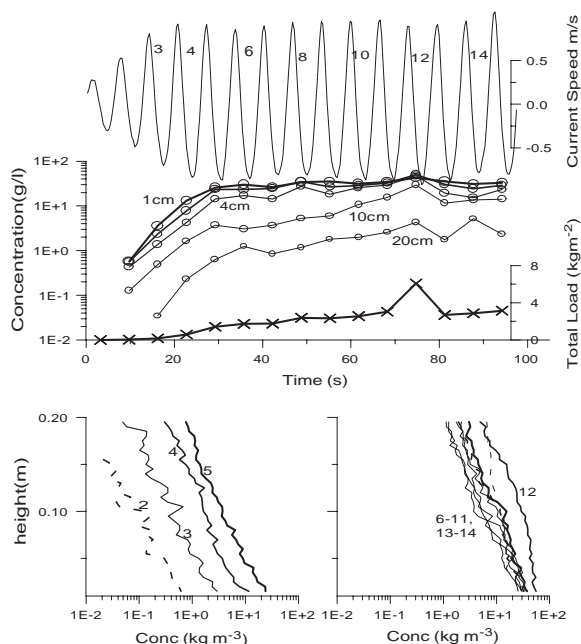


Fig. 3. Top: Current speed 0.75 m above the sand bed for the first 15 waves for Run MBB with  $H = 1.3$  m. Middle: Time series of wave-average concentrations at 1, 2, 4, 6, 10, 15 and 20 cm above the bed. Note the tendency for a one-wave lag at the lowest heights and a 2-or-more wave lag higher above the bed. Bottom: Sequence of wave-average concentration profiles showing the changes in the profile shape. Numbers refer to the waves in the top diagram.

### 3.2. Groupy waves

A 90 s-long wave group was selected from a water level time series of random waves with a relatively narrow spectral width of  $\gamma = 10$  (a JONSWAP spectrum has a  $\gamma$  of 3), and this group was repeated to provide a series of identical wave sets. The amplitude of the groups was varied, to produce five wave-group conditions with significant wave heights varying from 0.6 to 1.0 m. Additionally, the water depth was reduced from 4 to 3 m for the larger wave conditions to increase the orbital speeds close to the bed. As with the monochromatic waves, the groupy waves were run for two 30-min periods. Suspensions from the second 30-min period are presented here. The data have been analysed on a wave-by-wave basis through the wave group, but have first been ensemble-averaged over six sequential wave groups.

#### 3.2.1. Bedforms under the wave groups

The groupy waves were run during different experimental sequences and this has influenced the bedforms. Fig. 4 (top panel) shows the bed profiles from the mobile MTA; the measurement instruments were located at 106 m from the wave generator. The three runs with the lower water depth (GGA, GHA and GIA) were taken immediately after a sequence of wave runs at 9.1 s period designed to investigate suspension over flat beds and are characterised by a relatively smooth bed with occasional bedforms. The bed is unlikely to be in ‘equilibrium’ as the waves are groupy and have a range of orbital excursions; very little bedform development was observed over the period of these runs. Bedform development is clearly much slower than with monochromatic waves (Marsh et al., 1999). The other two runs were over steeper beds. GMB and GNB followed 4 h of ‘random’ waves ( $T = 6.5$ – $7.1$  s,  $H_s = 0.4$ – $1.25$  m) with bedforms of the order of 1 m wavelength and 0.1 m height.

#### 3.2.2. Development and decay of suspension by wave groups

The suspension of sand by the groupy waves shows the sediment being ‘pumped-up’ through the water column with the lag in concentration (relative to the forcing waves) increasing with height above the bed. The five wave conditions show similar features. Figs. 5 and 6 show details of two runs, GNB and GGA, one from each bed type. GNB and GGA have similar r.m.s. wave heights (0.73 and 0.77 m) but the water depths were different, resulting in different orbital current speeds of 0.50 and 0.63  $\text{ms}^{-1}$ . Despite the stronger orbital currents the suspended load during GGA (Fig. 6) was lower by a factor of 2–5 than GNB (Fig. 5). The local bedform characteristics are different between the two runs (Fig. 4 and Table 2) with the bedforms being almost twice as steep during GNB (weaker currents).

The concentration profiles are consistent with this difference in steepness. During GGA the profiles fit more closely to diffusive Rouse-type profiles suggesting sheet flow (the stronger wave orbital currents result in the partial washout of the ripples). The GNB profiles are more advective

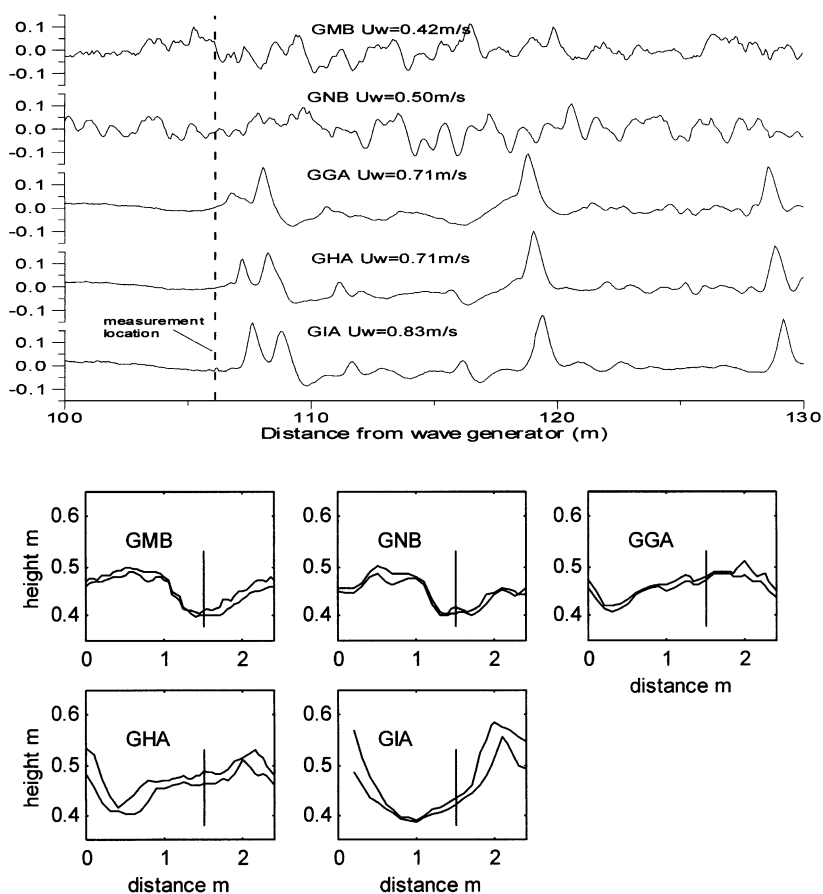


Fig. 4. Top panel: Bedforms along the centre of the wave channel for five group waves measured using the mobile MTA. Heights are in metres. The dashed vertical indicates the measurement location of the ABS ( $10^6 \text{ m}$  from the wave generator) Lower panels: Envelopes of the bed positions during the group wave measurements from the fixed MTA beneath the ABS sensors (the vertical line shows the ABS position).

(note the different scales on Figs. 5 and 6) and sediment is lifted higher into the water by vortex ejection. Green and Black (1998) noted similar patterns of suspension variation associated with hummocky bedforms when a thin ( $\sim 1 \text{ cm}$ ) carpet of suspension was observed over the slopes of the hummocks during the stronger currents under wave crest and trough, and clouds of sediment ejected from the “trenches” of the hummocks at flow reversal.

The structure of the wave-average sand concentration also reflects the differences in the seabed roughness. For the steeper bed GNB (Fig. 5) the lowest 4 cm of suspension follow the wave heights, responding rapidly to the wave-induced bed

stresses; above 0.1 m the concentration clearly lags the forcing. The maximum suspended load occurs at wave 12 (as wave heights start to decrease) and the profiles also become more uniform. This change in profile shape is consistent with a gradient in the size of the suspended sand with coarser sediment settling to the bed more quickly leaving finer material in suspension.

Over the ‘flatter’ bed (GGA) the concentration gradient is steeper and the suspension ‘carpet’ between the bed and 0.1 m increases in concentration from wave 7 to 12. Further from the bed (0.2 m), the concentration drops to a minimum at wave 10 before rising to its maximum at wave 12. The profiles change shape quickly as the wave

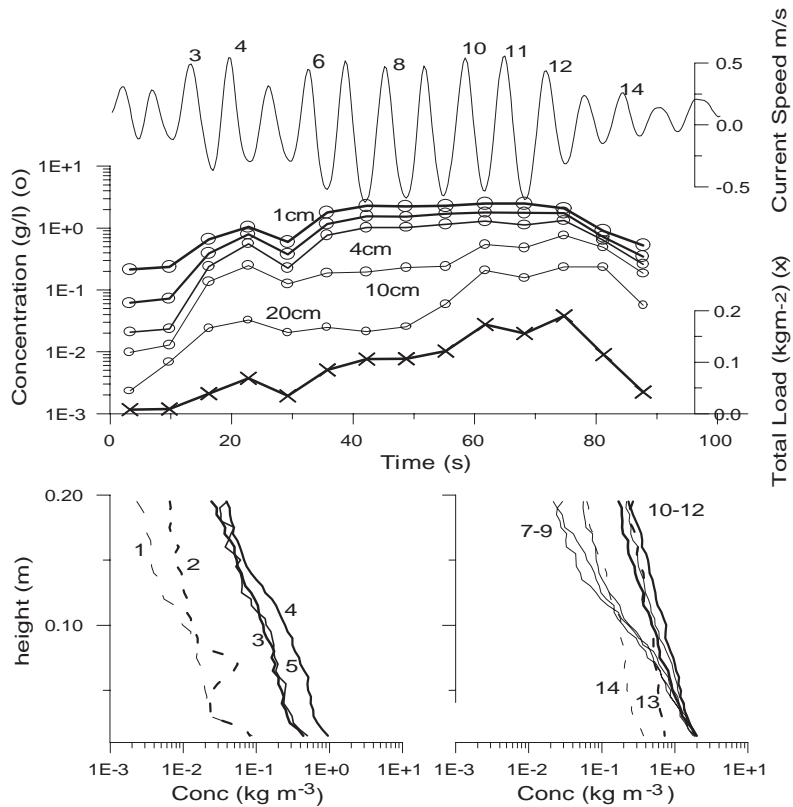


Fig. 5. Top: Current speed 0.75 m above the sand bed for the first fifteen waves in group GNB (rippled bed) with  $H = 0.73$  m and  $U_w = 0.50 \text{ ms}^{-1}$ . Middle: Time series of wave-average concentrations ( $\circ$ ) at 1, 2, 4, 10 and 20 cm above the bed and of the total suspended load ( $\times$ ). Bottom: Sequence of wave-average concentration profiles showing the changes in the profile shape. Numbers refer to the waves in the top diagram.

height drops, the suspension ‘carpet’ apparently expanding rapidly upwards at wave 12. The subsequent rapid decrease in concentration close to the bed (relative to the upper levels) is again consistent with a gradient in suspended size.

Villard et al. (1999, 2000) described the phenomena of a relatively uniform, high-concentration period as the wave heights in the group decreased. They suggested that this was associated with the ejection of vortices with alternating spin by flow over ripples that, with uniform waves, will tend to cancel each other out. As the waves decrease in height the vortex generated by the trough following a crest will be weaker than normal, resulting in the crest vortex decaying more slowly and maintaining more sediment in suspension. Our results are consistent with Villard

et al. (1999, 2000) in that three of the five groups given in Table 2 show maximum suspension at wave 12 while all five show a much more uniform suspension as the wave group decays.

### 3.2.3. Variability between groups

The pattern of suspended load is similar from group to group in any individual run but, as with the monochromatic waves, there is a large variability in the suspension caused by any particular wave in the group. While the height of an individual wave in the group has a standard deviation between 3% and 6.5%, the standard deviation of the suspended load due to an individual wave in the group varies between 25% and 41%.

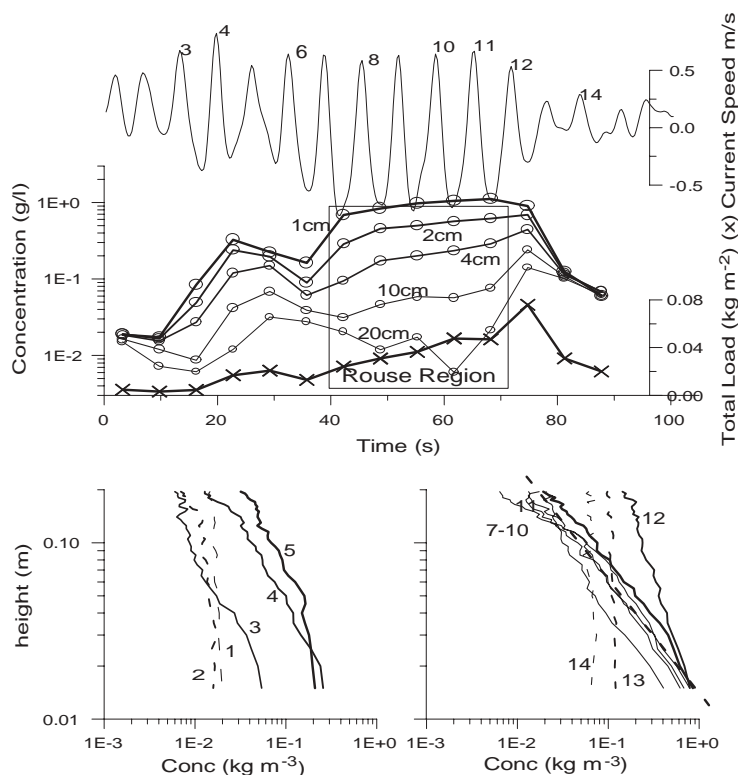


Fig. 6. Top: Current speed 0.75 m above the sand bed for the first fifteen waves in group GGA (flatter bed) with  $H = 0.77$  m and  $U_w = 0.63 \text{ m s}^{-1}$ . Middle: Time series of wave-average concentrations at 1, 2, 4, 6, 10, 15 and 20 cm above the bed. Bottom: Sequence of wave-average concentration profiles showing the changes in the profile shape. Numbers refer to the waves in the top diagram. Note the change in scale between this figure and Fig. 5.

Table 2

Water depths, wave heights and bedform dimensions for the 5 group waves. The wave orbital water speed is the first-order value computed using the rms wave height

Run ID	Depth (m)	$H$ (m) design	$H_{rms}$ (m)	$U_w$ ( $\text{m s}^{-1}$ )	Local MTA		Mobile MTA	
					$\lambda$ (m)	Ht (m)	$\lambda$ (m)	Steepness
GMB	4.75	0.6	0.62	0.42	2, 0.3	0.10, 0.02	1	0.16
GNB	4.75	0.7	0.73	0.50	2, 0.5	0.10, 0.02	1	0.20
GGA	3.75	0.7	0.77	0.63	2–3, 0.5	0.08, 0.02	—	0.11
GHA	3.75	0.8	0.87	0.71	2–3	0.12	—	0.12
GIA	3.75	0.9	1.02	0.83	2	0.17	—	0.13

#### 4. Modelling the sediment accumulation and decay processes

It would clearly be useful to quantify the effect of antecedent waves on the suspension associated

with any particular wave or wave group. Essentially the accumulation process is one of persistence, where the value of the suspension associated with the  $N$ th wave at any time  $t$  includes a term which is a function of the value of the suspension

due to previous waves at time  $t - nT$ , where  $T$  is the wave period. Rather than attempt to ‘model’ the development of the whole profile, we have chosen for simplicity to examine the vertically integrated suspended load  $W_N(t)$  (rather than, say, the reference concentration) as this parameter is representative of the whole profile. We use the most commonly used forcing variable, the Shields number  $\theta'$ , where the ‘prime’ indicates that the value is based on the skin friction. Alternatively, the Mobility Number could be used in place of the Shields number, with no substantive change to the conclusions. We also only consider wave-average values. The Shields number for a particular wave is given by

$$\theta' = \frac{0.5\rho_f' U^2}{(\rho_s - \rho)gD_{50}}, \quad (2)$$

where  $\rho$  is the water density,  $\rho_s$  is the sediment density,  $g$  is the acceleration due to gravity and  $D_{50}$  is the sediment diameter (50th percentile).  $U$  is the wave induced flow velocity above the wave boundary layer defined for each wave by  $U_{rms}$  over the period of the wave. The friction factor  $f_w'$  is that given by Swart (1974) for the sediment grains (skin friction)

$$f_w' = \exp[5.213(2.5D_{50}/A_w)^{0.194} - 5.977], \quad (3)$$

where  $A_w$  is the wave semi-excursion, all values again evaluated for each wave.

A very simple model has been chosen as our objective is to examine the importance of the pumping-up, and decay, to the suspension process rather than to explain all the features of the suspension. The model includes an entrainment (or pickup) constant  $C$ , excess Shields number raised to the power  $p$  and an exponential decay term applied to antecedent waves. The suspended load of the  $N$ th wave is given by

$$W_N = C(\theta(N) - \theta_{cr})^p + W_{N-1} \exp(-kT), \quad (4)$$

where  $T$  is the wave period,  $k$  is the rate of decay of the suspended load.  $\theta_{cr}$  is the critical Shields number at which general sand motion begins (Soulsby, 1997). Only the values of  $p$  more commonly used in suspension and sediment transport equations were considered ( $p = 1, 1.5, 2$  and  $3$ ).

An optimisation scheme was employed to fit the load predicted by the model  $\hat{W}_N$  to the measured suspension  $W_N$  for each of the 5 repeating wave groups given in Table 2, searching for the minimum absolute error (MAE) defined as  $1/n \sum_{Group} |W_N - \hat{W}_N|$  which, for positive  $C$  and  $k$ , is unique (it has no local minima). Two examples of the modelled suspended load compared to that measured are shown in Fig. 7. The dashed lines associated with the measured load show the variability (1 standard deviation) of the load, from group-to-group within the run. The modelled suspended load follows the general shape of the observed load with the exception of the large pulses of suspended sand that occur at exactly the same time in each group for any particular run (wave 12 in GNB, wave 11 in GIA). These pulses occurred in the same relative position (as wave height decreases) for 3 of the 5 wave groups. They may be due to the mechanism postulated by Villard et al. (1999, 2000) or due to advective effects associated with nearby bedforms. The values of the decay rates and the entrainment constant calculated from the optimisation procedure are shown in Fig. 8. With the exception of the lowest of the five wave groups (GMB) the decay rate is similar irrespective of the value of  $p$  chosen,  $0.061 \pm 0.013 \text{ s}^{-1}$ . The entrainment constant  $C$  on the other hand is more variable from run to run,  $0.038 \pm 0.039 \text{ kg m}^{-2} \text{ s}^{-1}$ , reflecting the different bedforms and measurement position relative to the bedforms. There was little difference in the lowest value of MAE whether  $p$  (the power to which the Shields number was raised) was 1.5, 2 or 3. Inclusion of the decay rate, compared to optimisation of the entrainment alone, reduces the MAE by a factor of 3.

The decay rate for the lowest wave group GMB is much larger than those of the other groups (Fig. 8). It is tempting to suggest that the decay rate increases as the wave height drops but we have no other data at lower wave heights to confirm this trend. There is some indication of a link between the entrainment rate and the position of the ABS relative to the bedforms. Both GMB and GNB, when the ABS was over the bedform trough, show high entrainment while GGA and GHA over the upper slopes of the bedforms are

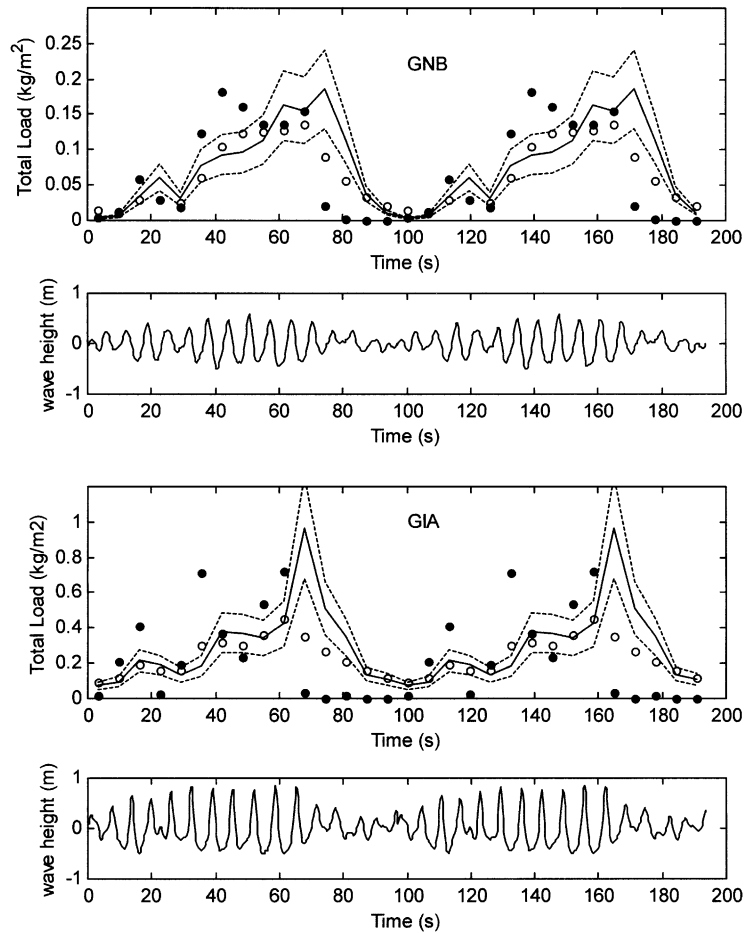


Fig. 7. The pump-up model (Eq. (5)) for the suspended load ( $\circ$ ), fitted to the measured load (solid line) using  $p = 2$ ,  $k = 0.076 \text{ s}^{-1}$  and  $C = 0.055 \text{ kg m}^{-2} \text{ s}^{-1}$  (GNB) and  $p = 3$ ,  $k = 0.042 \text{ s}^{-1}$  and  $C = 0.011 \text{ kg m}^{-2} \text{ s}^{-1}$  (GIA) using MAE optimization. The groups are repeated twice for clarity. The dashed lines show 1 standard deviation of the suspended load based on the variability of load from group-to-group. The solid dots are the total loads with no effects of antecedent waves included. The lower panels show the water level from the wave-wire.

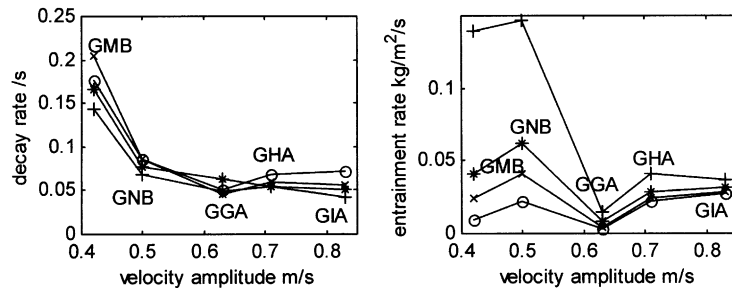


Fig. 8. The decay rate  $k$  ( $\text{s}^{-1}$ ) and the entrainment coefficient  $C$  ( $\text{kg m}^{-2} \text{ s}^{-1}$ ) from the MAE optimisation for the five repeating wave groups, plotted against the current speed for each group (see Table 2), for the  $p = 1$  ( $\circ$ ),  $1.5$  ( $\times$ ),  $2$  ( $*$ ) and  $3$  ( $+$ ).

Table 3

The results of applying the average decay rate of  $0.06\text{ s}^{-1}$  to independent wave records and optimising the entrainment, compared to values with no influence from antecedent waves

Run ID	Wave parameters $U_w$ ( $\text{m s}^{-1}$ ) $T$ (s)	No pump-up MAE entrainment ( $\text{kg m}^{-2}\text{ s}^{-1}$ )			Pump-up (decay = $0.061\text{ s}^{-1}$ ) MAE entrainment ( $\text{kg m}^{-2}\text{ s}^{-1}$ )		
		$p = 1.5$	$p = 2$	$p = 3$	$p = 1.5$	$p = 2$	$p = 3$
GAA	0.90, 6.5	0.127 <i>0.024</i>	0.131 <i>0.027</i>	0.139 <i>0.040</i>	0.080 <i>0.013</i>	0.081 <i>0.015</i>	0.088 <i>0.018</i>
RBB	0.75, 6.5	0.038 <i>0.011</i>	0.039 <i>0.015</i>	0.041 <i>0.017</i>	0.032 <i>0.0077</i>	0.029 <i>0.010</i>	0.027 <i>0.016</i>
DAA01	0.75, 7.2	0.035 <i>0.022</i>	0.038 <i>0.024</i>	0.044 <i>0.028</i>	0.023 <i>0.010</i>	0.022 <i>0.013</i>	0.023 <i>0.019</i>
DAB01	0.74, 7.2	0.020 <i>0.011</i>	0.023 <i>0.016</i>	0.026 <i>0.016</i>	0.012 <i>0.0064</i>	0.012 <i>0.0087</i>	0.013 <i>0.012</i>
DAB02	0.78, 7.2	0.037 <i>0.021</i>	0.040 <i>0.024</i>	0.044 <i>0.028</i>	0.024 <i>0.010</i>	0.024 <i>0.013</i>	0.027 <i>0.025</i>

much lower. GIA, on the other hand, does not support the trend.

Diagnostic models based on fitting parameters to individual data sets by minimising the MAE may be valueless in a prognostic situation. The decay rate has therefore been tested against the measured suspended loads during a variety of other wave conditions in the tank. Because of the large variability in the entrainment,  $C$ , it has been allowed to vary in these tests. The wave conditions used were as follows.

1. A wave group (GAA;  $H_{m0} = 1\text{ m}$ ,  $T = 6.5\text{ s}$ ), similar in shape and gamma value as those groups in the model calibration above, and run directly after the monochromatic waves discussed earlier. 6 wave groups were averaged.
2. A synthetic random wave series (RBB;  $H_{m0} = 0.9\text{ m}$ ,  $T = 6.5\text{ s}$ ). All waves in the series were used, with no averaging.
3. A wave series from 4 m water depth during the SANDYDUCK field experiment in 1997 (DAA, DAB;  $H_{m0} = 1.2\text{ m}$ ,  $T = 7.2\text{ s}$ ). Again, all waves in the series were used, with no averaging.

The wave conditions in the 3 cases above were relatively large so the model was tested using the average decay values obtained from the higher waves (i.e.  $k = 0.061\text{ s}^{-1}$ , excluding GMB) and three values of  $p$  (1.5, 2 and 3). In each case the

entrainment value was optimised. The predictive capacity (MAE) of the pump-up model was compared with that of a similar model with no pump-up (again optimising the entrainment).

In all three cases, the inclusion of pump-up produced significant decreases in the MAE (Table 3). There was little difference in the prognostic power of  $p = 1.5$ , 2 or 3. The model worked equally well for the random and SANDYDUCK waves (with no averaging) as for the group-averaged. The three values for the SANDYDUCK waves (DAA01, DAB01 and DAB02) correspond to three 10-min ABS records collected during 1 h of SANDYDUCK waves. The improvement in MAE for the groupy waves was 50% while that for the random was 25%. For the SANDYDUCK waves improvement ranged from 37% to 48%. The predicted and measured suspended-loads for two of these wave conditions, the random waves and one of the SANDYDUCK waves, are shown in Fig. 9.

## 5. Discussion and conclusions

Nielsen (1981) noted that there were distinct differences between the bedforms generated by regular (monochromatic) waves and those generated by spectral (natural) waves; with regular waves the bedforms were orbital (scaling to the

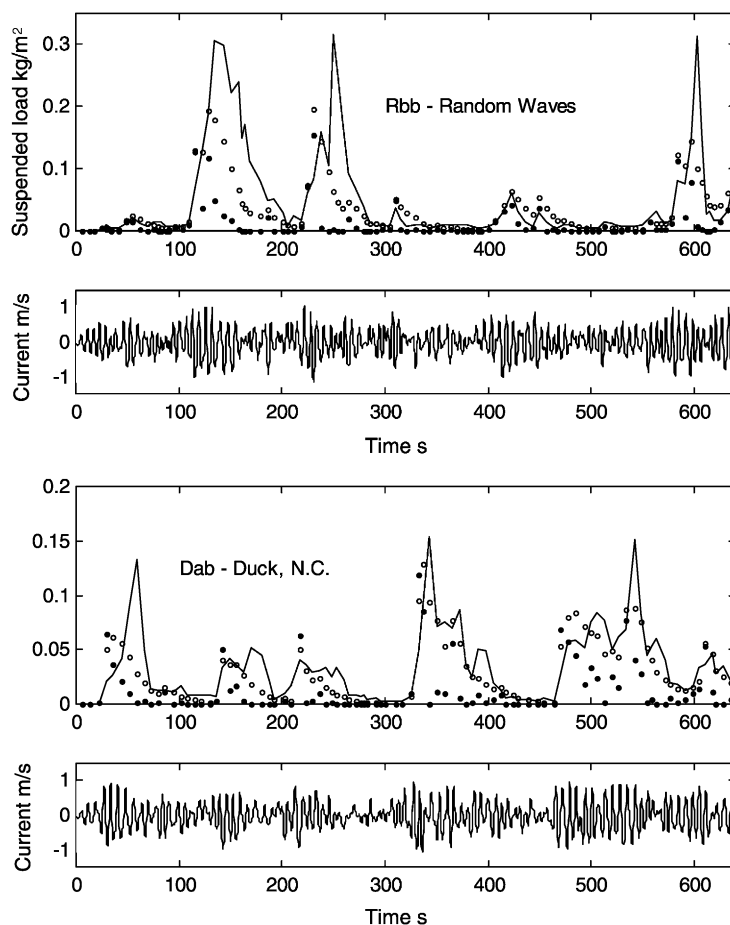


Fig. 9. The decay value of  $0.061 \text{ s}^{-1}$  tested on random waves (upper two panels) and waves from the 1997 SANDYDUCK field site (lower two panels) using  $p = 3$ . The predicted suspended concentration including the decay from previous waves is shown by the open circles; the filled circles are those predicted with no contribution from antecedent waves. The entrainment was optimised for each case.

near-bed wave excursion) while for spectral waves they were often anorbital. Marsh et al. (1999) were able to confirm, using measurements made under waves with various spectral widths, that bedforms rapidly scale to the orbital excursion when the waves are regular (every wave forcing the bed with the same length-scale) but bedforms tend to remain in their initial configuration, or evolve very slowly, when the waves consist of a variety of length-scales. This observation suggests that the small number of waves in a wave spectrum which scale with the *existing* bedforms are more effective at maintaining the existing bedforms than are a larger number of waves at changing the bedforms,

particularly when there is no clearly defined new length-scale.

These experiments support the results of Nielsen (1981) and Marsh et al. (1999). Bedforms rapidly scaled to the orbital excursion of the regular waves (Fig. 1). It is therefore likely that the bedforms generated in this wave channel are in equilibrium (after the initial 30-min run) with the monochromatic waves. For group and random waves equilibrium with the waves is less likely and bedform dimensions are defined more by antecedent (pre-existing) bedforms (Fig. 4). In terms of the suspended sediment profiles and suspended load (Fig. 8 and Table 3) this unsteady bed state

will tend to give more variable results but is probably more typical of ‘natural’ conditions.

The pumping-up of sediment is immediately apparent from the concentration time-series under monochromatic, groupy and random waves, confirming earlier field observations (e.g. Hanes, 1991; Villard et al., 1999, 2000). The simple antecedent-wave model proposed here (Eq. (4)), based on the skin friction Shields number, an entrainment constant and a rate of turbulent decay from antecedent waves, is able to explain considerably more of the observed suspended load than a similar model without the decay term (a factor of 3 for the calibration runs). In terms of the efficacy of the model, measured by the MAE, there was little to choose between the different powers ( $p = 1.5, 2$  or  $3$ ) to which the Shields number was raised. Using the average decay rate  $0.061 \text{ s}^{-1}$  from the four higher groups (Fig. 8) and optimising the entrainment constant the model was able to produce a factor of 1.3–2 improvement in the MAE when tested on a number of independent wave conditions, including ‘real’ waves from SANDYDUCK.

Two types of suspended load variability were noted here. The first is the variation due to bedform height, shape and measurement location that results in the wide spread of entrainment constants (an order of magnitude) seen in Fig. 8 and in Table 3. The second is the variability that occurs between waves of a similar height over the same bedforms, e.g. the variability of  $\pm 30\%$  in the suspension due to a sequence of regular waves that have a variability in height of only  $\pm 4\%$ , and the variability in suspension  $\pm 25\text{--}41\%$  between waves in the repeating wave groups. This variability suggests that even with good knowledge of the bedforms, sediment characteristics, etc., we are unlikely to be able to predict the suspension due to any individual wave to better than about 30% and, in the natural environment where our knowledge of the bedforms is rarely good, we should not expect to predict better than a factor of two at best. We view this fact as fundamentally linked to the stochastic nature of turbulence.

The average decay rate of  $0.061 \text{ s}^{-1}$  indicates a decay time scale of approximately 16 s, which is rather large considering the fall velocity of the

sand. Using the median measured fall velocity of  $3.6 \text{ cm s}^{-1}$ , the settling length scale corresponding to a time scale of 16 s would be approximately 60 cm. This is much greater than the typical vertical length scale of the suspension, which is mainly contained in the region  $< 10 \text{ cm}$  above the seabed. This raises interesting questions regarding the effects of turbulence upon the fall velocity of the sand, as well as basic questions regarding the time scales for the decay of turbulence in the field. Both of these issues seem suitable for investigation using numerical simulations of particles in a wave-forced field of turbulence.

While the inclusion of the effects of antecedent waves via a decay rate of  $0.061 \text{ s}^{-1}$  gives significant improvement in the predicted suspended load time series, it is clear that this is not the full story. Villard et al. (1999, 2000) noted that there was a burst of higher-than-expected suspension towards the end of the wave group, as the wave height rapidly decreased. A similar effect is seen in our data with three of the five repeating wave groups (see GGA, GIA and GNA in Figs. 5–7) exhibiting the highest wave-average suspended concentration just after the waves begin to decrease in height. This ‘decay burst’, which can also be seen in the suspension under random waves (Fig. 9, Rbb  $t = 130, 250$  and  $600 \text{ s}$ ) and in the data from SANDYDUCK (Fig. 9, Dab,  $t = 55, 330$  and  $530 \text{ s}$ ), cannot be explained by a simple antecedent-wave (pumping and decay) model. However, the process by which it occurs is clearly important as it contributes significantly to the total suspended load.

## Acknowledgements

The experiments were made possible by the University of Hannover and FZK through the Human Capital and Mobility Program of the EU and by the NICOP and Coastal Sciences Program of the US Office of Naval Research. We would also like to thank our colleagues, particularly Marjolein Dohman-Jensen, Jan Ribberink, Charlotte Obhrai, Jon Taylor and Steve McLean for their assistance in the work at Hannover and the staff of the FZK facility.

## References

- Grant, W.D., Madsen, O.S., 1982. Movable bed roughness in unsteady oscillatory flow. *Journal of Geophysical Research* 87, 469–481.
- Green, M.O., Black, K.P., 1998. Suspended sediment reference concentration under waves: field observations and critical analysis of two predictive models. *Coastal Engineering* 38, 115–141.
- Green, M.O., Dolphin, A., Swales, A., Vincent, C.E., 1999. Transport of mixed-size sediments in a tidal channel. *Coastal Sediments*.
- Hanes, D.M., 1991. Suspension of sand due to wave groups. *Journal of Geophysical Research* 96 (C5), 8911–8915.
- Hanes, D.M., Alymov, V., Chang, Y., Jette, C.D., 2001. Wave formed sand ripples at Duck, North Carolina. *Journal of Geophysical Research* 106 (C10), 22575.
- Jette, C.D., Hanes, D.M., 1997. High resolution sea-bed imaging: an acoustic multiple transducer array. *Measurement Science and Technology* 8, 787–792.
- Marsh, S.W., Vincent, C.E., Osborne, P.D., 1999. Bedforms in a laboratory wave flume: an evaluation of predictive models for bedform wavelengths. *Journal of Coastal Research* 15 (3), 624–634.
- Miller, M.C., Komar, P.D., 1980. A field investigation of the relationship between oscillation ripple-spacing and near-bottom water orbital motions. *Journal of Sedimentary Petrology* 50 (1), 183–191.
- Nielsen, P., 1981. Dynamics and geometry of wave-generated ripples. *Journal of Geophysical Research* 86 (C7), 6467–6472.
- Nielsen, P., 1992. Combined convection-diffusion modelling of sediment entrainment. *Proceedings of the 23rd International Conference on Coastal Engineering, Venice*, pp. 3202–3215.
- Ribberink, J.S., Dohmen-Janssen, C.M., Hanes, D.M., McLean, S.R., Taylor, J.A., Vincent, C., 2000. Near-bed sand transport mechanisms under waves: large-scale flume experiments. In: *Twenty-seventh International Conference on Coastal Engineering, ASCE, Sydney, Australia, July 16–21, 2000*.
- Soulsby, R., 1997. *Dynamics of Marine Sands*. Thomas Telford.
- Swart, D.H., 1974. Offshore sediment transport and equilibrium beach profiles. *Delft Hydraulics Laboratory Publication* 131, 87pp.
- Villard, P.V., Osborne, P.D., Vincent, C.E., 1999. Influence of wave groups on sand re-suspension over bedforms in a large scale wave flume. *Proceedings of the Fourth International Symposium on Coastal Engineering and Science of Coastal Sediment Processes CS99, New York*, pp. 367–376.
- Villard, P.V., Osborne, P.D., Vincent, C.E., 2000. Influence of wave groups on SSC patterns over vortex ripples. *Continental Shelf Research* 20, 2391–2410.
- Vincent, C.E., Marsh, S.W., Webb, M.P., Osborne, P.D., 1999. Spatial and temporal structures of suspension and transport over mega-ripples on the shore face. *Journal of Geophysical Research* 104, 11215–11224.